

John A. Nairn¹, Yung Ching Liu¹, and Costas Galiotis²

Analysis of Stress Transfer from the Matrix to the Fiber Through an Imperfect Interface: Application to Raman Data and the Single-Fiber Fragmentation Test

REFERENCE: Nairn, J. A., Liu, Y. C., and Galiotis, C., “Analysis of Stress Transfer from the Matrix to the Fiber Through an Imperfect Interface: Application to Raman Data and the Single-Fiber Fragmentation Test,” *Fiber, Matrix, and Interface Properties, ASTM STP 1290*, Christopher J. Spragg and Lawrence T. Drzal, Eds., American Society for Testing and Materials, 1996, pp. 47–65.

ABSTRACT: A new analysis for stress transfer from the fiber to the matrix through an imperfect interface was derived using a Bessel-Fourier series. The new analysis is specific for the fragmentation test. It satisfies equilibrium and compatible every place and satisfies most boundary conditions exactly. The only approximation is the axial stress boundary condition in the fiber which is satisfied in an averaged sense instead of exactly. Two important advantages of the stress transfer analysis are that it can analyze anisotropic fibers and it can include imperfect interfaces or interphases. Theoretical predictions of stress stress transfer were compared to experimental Raman spectroscopy results. The predictions agree well experiments and they can be used to measure interface properties. The stress transfer analysis was coupled with an interfacial failure criterion to model the fragmentation test. The results of modeling fragmentation data as a function of applied strain suggested new ways of interpreting fragmentation experiments and cast doubt on the relevance of the commonly measured interfacial shear strength.

KEY WORDS: composites, stress transfer, Raman spectroscopy, fragmentation test, imperfect interface, interphase, Bessel functions, axisymmetric stress analysis

In the single-fiber fragmentation test, a single fiber is embedded in a matrix and loaded in tension until the fiber fractures into fragments [1–6]. The average fragment length and the distribution of fragment lengths as a function of applied strain tell us something about the fiber/matrix interface. But the question remains: what do the results tell us about the interface? Furthermore, which experimental results do we need? How do we interpret those results? This paper discusses a new stress analysis for stress transfer from the matrix to the fiber in a fragmentation specimen. We use the analysis to model the fragmentation test and to make suggestions about interpreting fragmentation test results.

At the first fiber break in a fragmentation test, the axial stress in the fiber is zero. Stress transfer across the interface permits stress to return to the fiber which permits additional fiber breaks with continued loading. The fragmentation process ceases when there is insufficient stress transfer over the length of a fragment for the stress to reach the strength of the fiber. To interpret the fragmentation test we must analyze the process of stress transfer from the matrix to the fiber. One analysis method is to assume an elastic-plastic

¹Associate Professor and Graduate Student, respectively, Material Science and Engineering, University of Utah, Salt Lake City, Utah 84112, USA

²University of London, Queen Mary and Westfield College, Mile End Road, London E1 4NS, UK

interface [7]. In the post yield condition the interface is assumed to have a constant shear stress and therefore a linear rate of stress transfer into the fiber. With this model, the critical fragment length, or the length when the fragmentation process ceases, is easily calculated to be [7]

$$l_c = \frac{\sigma_f(l_c)r_1}{\tau_{ic}} \quad (1)$$

where $\sigma_f(l_c)$ is the strength of the fiber for specimens of length equal to the critical length, r_1 is the fiber radius, and τ_{ic} is the critical interfacial shear stress. This elastic-plastic model is sometimes incorporated into a two-zone model with a constant shear stress or frictional stress in the yield zone and elastic stress transfer through a perfect interface in the undamaged zone (*e.g.*, Ref. [8]). The elastic stress transfer part is analyzed by one-dimensional, shear-lag methods. We suggest these models are too simplistic. The assumption of a constant interfacial shear stress is unrealistic for many interfaces. The one-dimensional methods give no information about radial stress and thus do a poor job of accounting for thermal stresses and frictional effects. Finally, these models only give qualitative measures of interface properties (*e.g.*, τ_{ic}) which are of limited practical use when the goal is to predict the role of the interface in real laminates.

The first, three-dimensional, axisymmetric analyses of stress transfer from a rod to an elastic medium were done by Muki and Sternberg [9–11]. They treated the matrix as a three-dimensional elastic continuum. The fiber is reduced to a fictitious one-dimensional reinforcement over the cross-section of the actual fiber. They reduced the resulting problem to an integro-differential equation that could be solved numerically. Since their original paper, the method of replacing the fiber by a one-dimensional reinforced continuum has been widely used (*e.g.*, Refs. [12–16]). Unfortunately, the method is not suitable for the fragmentation test. Instead of transfer from a single break to an elastic medium, we want to analyze stress transfer in the presence of periodic cracks. Instead of isotropic fibers, we want to analyze anisotropic fibers such as carbon fibers or aramid fibers. Finally, replacing the fiber by a one-dimensional reinforced continuum blurs the interface. This blurring gives poor results about interfacial stresses [11] and makes it difficult to model an imperfect interface.

In this paper we give a three-dimensional axisymmetric analysis of the fragmentation test by using Bessel-Fourier series stress functions. The new analysis is nearly exact. It obeys equilibrium and compatibility every place. It obeys all boundary conditions except one. The single approximation is that instead of the fiber axial stress being exactly zero at the fiber break, only the average axial fiber stress is equal to zero. Some advantages of the analysis are that it can handle anisotropic fibers, it can model an imperfect interface, and it gives explicit results for all components of stress along the interface. After outlining the derivation of the stress analysis, the predictions are compared to direct experimental results of stress transfer using Raman spectroscopy. The experiments and predictions agree well. Finally, we used the analysis and a simple model for interfacial damage to model the fragmentation tests. The results of the modeling led to suggestions about conducting and interpreting fragmentation experiments

Stress Analysis

Stress Function Approach

Figure 1 shows the boundary conditions for analysis of the fragmentation specimen. Figure 1A shows a fragmentation specimen. A single fragment from that specimen is magnified in FIG. 1B. Because the fiber is broken at the two ends of the fragment, the axial stress (σ_{zz}) and shear stress (τ_{rz}) on the fiber must be zero. By continuity of displacement from one fragment zone to the next, the axial displacement (w) in the matrix at the fragment ends must be a constant or independent of r . Symmetry dictates that the shear stress (τ_{rz}) in the matrix at the fragment ends must be zero. Finally, the entire specimen is subjected to a temperature differential of $T = T_s - T_0$ where T_s is the specimen temperature and T_0 is the stress-free temperature.

For convenience, we divide the problem into two problems illustrated in Figs. 1C and 1D. Figure 1C shows the far-field problem or the stresses for an infinitely long transversely isotropic cylinder embedded in an infinite matrix while the matrix is under an axial load of σ_0 and temperature differential of T . The boundary conditions are:

$$\sigma_{zz,2}(\pm l/2) = \sigma_0 \quad \tau_{rz,1}(\pm l/2) = \tau_{rz,2}(\pm l/2) = 0 \quad w_1(\pm l/2) = w_2(\pm l/2) = \pm \frac{l}{2} \left(\frac{\sigma_0}{E_m} + \alpha_m T \right) \quad (2)$$

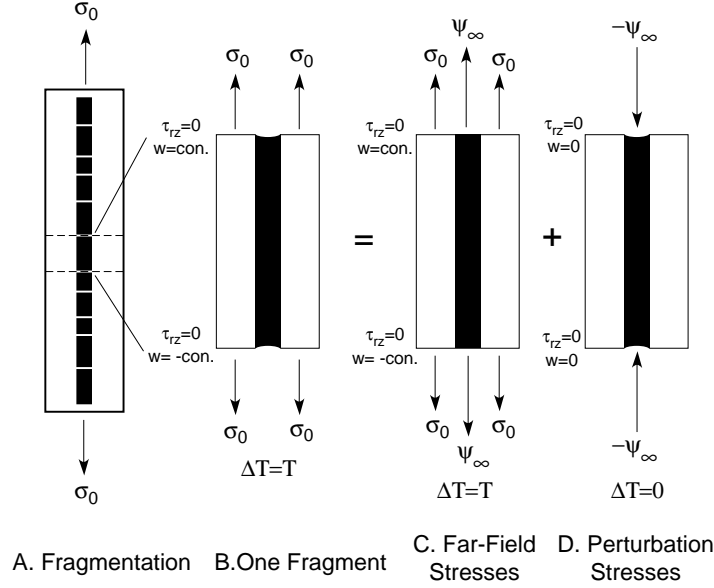


FIG. 1 — *A.* In the fragmentation test, a single fiber embedded in a large amount of matrix fragments into multiple small fragments. *B.* The boundary conditions on a cell containing a single fiber fragment of length l extending from $z = -l/2$ to $z = +l/2$. $\sigma_{zz,1} = 0$ on the fiber ends; $\tau_{rz,1} = \tau_{rz,2} = 0$ at $z = \pm l/2$; w_2 at $z = \pm l/2$ is constant (“ \pm con.”) or independent of r ; the temperature differential is T . *C.* The far-field stresses are the stresses for an infinitely long, unbroken fiber in an infinite matrix under an applied stress of σ_0 and temperature differential T . *D.* For perturbation stresses, $\sigma_{zz,1} = -\psi_\infty$ on the fiber ends; $\tau_{rz,1} = \tau_{rz,2} = 0$ at $z = \pm l/2$; $w_2 = 0$ at $z = \pm l/2$; the temperature differential is 0.

The form of the far-field stresses is

$$\begin{aligned} \sigma_{zz,1} &= \psi_\infty & \sigma_{rr,1} &= \sigma_\infty & \sigma_{\theta\theta,1} &= \sigma_\infty & \tau_{rz,1} &= 0 \\ \sigma_{zz,2} &= \sigma_0 & \sigma_{rr,2} &= \frac{r_1^2 \sigma_\infty}{r^2} & \sigma_{\theta\theta,2} &= -\frac{r_1^2 \sigma_\infty}{r^2} & \tau_{rz,2} &= 0 \end{aligned} \quad (3)$$

where subscripts “1” and “2” refer to the fiber and the matrix, respectively, and r_1 is the radius of the fiber. By equating axial strains and the interfacial radial displacements in the fiber and matrix, it is easy to solve for the constants ψ_∞ and σ_∞ :

$$\psi_\infty = \frac{\left(\frac{2\nu_A \nu_m}{E_A} - \frac{1-\nu_T}{E_T} - \frac{1+\nu_m}{E_m} \right) \frac{E_A \sigma_0}{E_m} + \left(\frac{2\nu_A}{E_A} (\alpha_T - \alpha_m) + \left(\frac{1-\nu_T}{E_T} + \frac{1+\nu_m}{E_m} \right) (\alpha_A - \alpha_m) \right) E_A T}{\frac{2\nu_A^2}{E_A} - \frac{1-\nu_T}{E_T} - \frac{1+\nu_m}{E_m}} \quad (4)$$

$$\sigma_\infty = \frac{-(\nu_A - \nu_m) \frac{\sigma_0}{E_m} + (\nu_A (\alpha_A - \alpha_m) + (\alpha_T - \alpha_m)) T}{\frac{2\nu_A^2}{E_A} - \frac{1-\nu_T}{E_T} - \frac{1+\nu_m}{E_m}} \quad (5)$$

where E is modulus, ν is Poisson’s ratio, and α is thermal expansion coefficient. The subscripts A and T refer to axial and transverse properties of the transversely isotropic fiber. The subscript m refers to properties of the isotropic matrix.

Figure 1D shows the harder problem—the perturbation stresses. Here the matrix ends have zero shear stress and zero axial displacement. The fiber ends are also under zero shear stress but have a compressive axial stress of $-\psi_\infty$. Because temperature differential is included in the far-field stresses, the stress analysis for the perturbation stresses uses $T = 0$. The boundary conditions are:

$$\sigma_{zz,1}(\pm l/2) = -\psi_\infty \quad \tau_{rz,1}(\pm l/2) = \tau_{rz,2}(\pm l/2) = 0 \quad w_1(\pm l/2) = w_2(\pm l/2) = 0 \quad (6)$$

We define $\vec{\sigma}_{0,i}$ as the far-field stresses in component i ($i = 1$ or 2) and $\vec{\sigma}_{p,i}$ as the perturbation stresses in component i due to unit compression on the fiber; then, by superposition, the stresses in the fragment in FIG. 1B are $\vec{\sigma}_i = \vec{\sigma}_{0,i} + \psi_\infty \vec{\sigma}_{p,i}$. We now proceed to find $\vec{\sigma}_{p,i}$.

From Lekhnitskii [17], the stresses and displacements for an axisymmetric stress state in a transversely isotropic fiber can be written as

$$\sigma_{rr} = -\frac{\partial}{\partial z} \left(\frac{\partial^2 \Psi}{\partial r^2} + \frac{b}{r} \frac{\partial \Psi}{\partial r} + a \frac{\partial^2 \Psi}{\partial z^2} \right) \quad (7)$$

$$\sigma_{\theta\theta} = -\frac{\partial}{\partial z} \left(b \frac{\partial^2 \Psi}{\partial r^2} + \frac{1}{r} \frac{\partial \Psi}{\partial r} + a \frac{\partial^2 \Psi}{\partial z^2} \right) \quad (8)$$

$$\sigma_{zz} = \frac{\partial}{\partial z} \left(c \frac{\partial^2 \Psi}{\partial r^2} + \frac{c}{r} \frac{\partial \Psi}{\partial r} + d \frac{\partial^2 \Psi}{\partial z^2} \right) \quad (9)$$

$$\tau_{rz} = \frac{\partial}{\partial r} \left(\frac{\partial^2 \Psi}{\partial r^2} + \frac{1}{r} \frac{\partial \Psi}{\partial r} + a \frac{\partial^2 \Psi}{\partial z^2} \right) \quad (10)$$

$$u = \frac{b-1}{2G_T} \frac{\partial^2 \Psi}{\partial r \partial z} \quad (11)$$

$$w = \frac{1}{G_A} \left(\frac{\partial^2 \Psi}{\partial r^2} + \frac{1}{r} \frac{\partial \Psi}{\partial r} \right) + \frac{(d+2\nu_A a)}{E_A} \frac{\partial^2 \Psi}{\partial z^2} \quad (12)$$

where u is radial displacement and the constants are

$$a = \frac{-\nu_A(1+\nu_T)}{1 - \frac{\nu_A^2 E_T}{E_A}} \quad (13)$$

$$b = \frac{\nu_T - \frac{\nu_A E_T}{E_A} \left(\frac{E_A}{G_A} - \nu_A \right)}{1 - \frac{\nu_A^2 E_T}{E_A}} \quad (14)$$

$$c = \frac{\frac{E_A}{G_A} - \nu_A(1+\nu_T)}{1 - \frac{\nu_A^2 E_T}{E_A}} \quad (15)$$

$$d = \frac{\frac{E_A}{2G_T}(1-\nu_T)}{1 - \frac{\nu_A^2 E_T}{E_A}} \quad (16)$$

where G is shear modulus. The stress function Ψ must satisfy the equation

$$\nabla_1^2 \nabla_2^2 \Psi = 0 \quad (17)$$

where the operators are defined by

$$\nabla_i^2 = \frac{\partial^2}{\partial r^2} + \frac{1}{r} \frac{\partial}{\partial r} + \frac{1}{s_i^2} \frac{\partial^2}{\partial z^2} \quad (18)$$

and the constants, s_1 and s_2 are

$$s_1^2 = \frac{a+c + \sqrt{(a+c)^2 - 4d}}{2d} \quad (19)$$

$$s_2^2 = \frac{a+c - \sqrt{(a+c)^2 - 4d}}{2d} \quad (20)$$

The hoop displacement (v) and the unspecified shear stresses ($\tau_{r\theta}$ and $\tau_{\theta z}$) are zero in axisymmetric stress states. For an isotropic matrix, these equations reduce to the well-known result in Love [18]:

$$\sigma_{rr} = \frac{\partial}{\partial z} \left(\nu_m \nabla^2 \chi - \frac{\partial^2 \chi}{\partial r^2} \right) \quad (21)$$

$$\sigma_{\theta\theta} = \frac{\partial}{\partial z} \left(\nu_m \nabla^2 \chi - \frac{1}{r} \frac{\partial \chi}{\partial r} \right) \quad (22)$$

$$\sigma_{zz} = \frac{\partial}{\partial z} \left((2 - \nu_m) \nabla^2 \chi - \frac{\partial^2 \chi}{\partial z^2} \right) \quad (23)$$

$$\tau_{rz} = \frac{\partial}{\partial r} \left((1 - \nu_m) \nabla^2 \chi - \frac{\partial^2 \chi}{\partial z^2} \right) \quad (24)$$

$$u = -\frac{1}{2G} \frac{\partial^2 \chi}{\partial r \partial z} \quad (25)$$

$$w = \frac{1}{2G} \left[2(1 - \nu_m) \nabla^2 \chi - \frac{\partial^2 \chi}{\partial z^2} \right] \quad (26)$$

where the equation for χ is

$$\nabla^4 \chi = 0 \quad (27)$$

We begin by stating stress functions for the fiber and matrix that solve the perturbation stresses in the fragmentation specimen almost exactly. The stress functions in the fiber (Ψ) and the matrix (χ) for a fragment of length l with the origin for $z = 0$ at the center of the fragment are

$$\Psi = A_{30}z^3 + A_{32}r^2z + \frac{A_{50}}{c} \left(cz^5 + \frac{15ad}{8}r^4z - 5dr^2z^3 \right) + \sum_{i=1}^{\infty} \sin k_i z (b_{1i}I_0(\beta_{1i}r) + b_{2i}I_0(\beta_{2i}r)) \quad (28)$$

$$\chi = A_1z \ln r + \sum_{i=1}^{\infty} \sin k_i z (a_{0i}K_0(k_i r) + a_{1i}k_i r K_1(k_i r)) \quad (29)$$

where A_{ij} , A_1 , b_{ji} , and a_{ji} are undetermined constants,

$$k_i = \frac{2i\pi}{l} \quad \text{and} \quad \beta_{ji} = \frac{k_i}{s_j} \quad (30)$$

Both the fiber and matrix stress functions contain a Bessel-Fourier series. The fiber stress function has modified Bessel functions of the first kind ($I_0(x)$); the matrix stress function has modified Bessel functions of the second kind ($K_0(x)$ and $K_1(x)$). The fiber has only modified Bessel functions of the first kind, because the second kind diverge as r approaches 0; the matrix has only modified Bessel functions of the second kind because the first kind diverge as r approaches ∞ . The Fourier series include only $\sin k_i z$ terms due to symmetry about $z = 0$.

In deriving the stress functions, we started with the Bessel-Fourier series terms. Bessel-Fourier series are a well-known method for analysis of cylinders with arbitrary transverse loading [18], but, by themselves they cannot solve the fragmentation problem. If they are used by themselves, the only possible solution is one that vanishes identically. We traced this problem to the substitution of Fourier series into equations involving derivatives (*e.g.*, Eqs (7)–(12)). Unfortunately, the derivative of a Fourier series is not necessarily the Fourier series of the derivative of that function. In particular, stress functions based *only* on a Bessel-Fourier series will never recover components of the stress state that are independent of z . To compensate for this deficiency, we added more terms to the stress function. The leading terms in Eqs (28) and (29) were selected because they provide the desired z -independent components to the stresses and they are consistent with the boundary conditions. The leading terms in the fiber are based on the polynomial stress functions described by Lekhnitskii [17]. We choose polynomial stress functions including terms up to z^5 . The final form of the additional terms in the fiber stress function is dictated by symmetry and by a requirement that the shear stress at $z = \pm l/2$ remains zero. The leading terms in the matrix stress function were chosen to give z -independent normal stresses and zero shear stress.

In the interest of brevity, we will not explicitly state all stresses, strains, and displacements. Instead, we only state the ones needed to reproduce the results in this paper — the axial stresses, shear stresses, radial stresses, axial strains, and radial displacements in the fiber and matrix:

$$\sigma_{zz,1} = B_2 + B_3 d \xi^2 + \sum_{i=1}^{\infty} \cos k_i \zeta \left[b_{1i} \left(\frac{c}{s_1^2} - d \right) I_0(\beta_{1i} \xi) + b_{2i} \left(\frac{c}{s_2^2} - d \right) I_0(\beta_{2i} \xi) \right] \quad (31)$$

$$\tau_{rz,1} = \sum_{i=1}^{\infty} \sin k_i \zeta \left[b_{1i} \left(\frac{1}{s_1^2} - a \right) \frac{I_1(\beta_{1i} \xi)}{s_1} + b_{2i} \left(\frac{1}{s_2^2} - a \right) \frac{I_1(\beta_{2i} \xi)}{s_2} \right] \quad (32)$$

$$\sigma_{rr,1} = B_1 - B_3 \left[\frac{(1 + \nu_T) \rho^2}{3} + \frac{(1 - \nu_T) a}{4} \xi^2 \right] + \sum_{i=1}^{\infty} \cos k_i \zeta \left[-B_3 (-1)^i \frac{4(1 + \nu_T)}{k_i^2} + b_{1i} \left(\left(a - \frac{1}{s_1^2} \right) I_0(\beta_{1i} \xi) \right. \right.$$

$$\left. + \frac{(1-b) I_1(\beta_{1i}\xi)}{s_1^2 \beta_{1i}\xi} \right) + b_{2i} \left(\left(a - \frac{1}{s_2^2} \right) I_0(\beta_{2i}\xi) + \frac{(1-b) I_1(\beta_{2i}\xi)}{s_2^2 \beta_{2i}\xi} \right) \right] \quad (33)$$

$$\begin{aligned} \varepsilon_{zz,1} &= \frac{\partial w_1}{\partial \zeta} = -\frac{2\nu_A}{E_A} B_1 + \frac{1}{E_A} B_2 + \frac{B_3}{2G_T} \left[(1-\nu_T)\xi^2 + \frac{2\nu_A E_T \rho^2}{3E_A} \right] + \sum_{i=1}^{\infty} \cos k_i \zeta \left[B_3 (-1)^i \frac{8\nu_A (1+\nu_T)}{E_A k_i^2} \right. \\ &\quad \left. + b_{1i} \left(\frac{1}{s_1^2 G_A} - \frac{d+2\nu_A a}{E_A} \right) I_0(\beta_{1i}\xi) + b_{2i} \left(\frac{1}{s_2^2 G_A} - \frac{d+2\nu_A a}{E_A} \right) I_0(\beta_{2i}\xi) \right] \end{aligned} \quad (34)$$

$$\begin{aligned} u_1 &= \xi \left(\frac{1-\nu_T}{E_T} B_1 - \frac{\nu_A}{E_A} B_2 \right) + \frac{B_3 (1-\nu_T)}{2G_T} \left(\frac{a\xi^3}{4} - \frac{\xi\rho^2}{3} \right) + \frac{1}{2G_T} \sum_{i=1}^{\infty} \cos k_i \zeta \left[-B_3 (-1)^i \frac{4(1-\nu_T)\xi}{k_i^2} \right. \\ &\quad \left. + \frac{b_{1i}(b-1) I_1(\beta_{1i}\xi)}{s_1^2 \beta_{1i}} + \frac{b_{2i}(b-1) I_2(\beta_{2i}\xi)}{s_2^2 \beta_{2i}} \right] \end{aligned} \quad (35)$$

$$\sigma_{zz,2} = \sum_{i=1}^{\infty} \cos k_i \zeta \left[a_{0i} K_0(k_i \xi) + a_{1i} (k_i \xi K_1(k_i \xi) - 2(2-\nu_m) K_0(k_i \xi)) \right] \quad (36)$$

$$\tau_{rz,2} = \sum_{i=1}^{\infty} \sin k_i \zeta \left[a_{0i} (-K_1(k_i \xi)) + a_{1i} (2(1-\nu_m) K_1(k_i \xi) - k_i \xi K_0(k_i \xi)) \right] \quad (37)$$

$$\sigma_{rr,2} = \frac{A_1}{\xi^2} + \sum_{i=1}^{\infty} \cos k_i \zeta \left[a_{0i} \left(-K_0(k_i \xi) - \frac{K_1(k_i \xi)}{k_i \xi} \right) + a_{1i} ((1-2\nu_m) K_0(k_i \xi) - k_i \xi K_1(k_i \xi)) \right] \quad (38)$$

$$w_2 = \frac{1}{2G_m} \sum_{i=1}^{\infty} \frac{\sin k_i \zeta}{k_i} \left[a_{0i} K_0(k_i \xi) + a_{1i} (k_i \xi K_1(k_i \xi) - 4(1-\nu_m) K_0(k_i \xi)) \right] \quad (39)$$

$$\varepsilon_{zz,2} = \frac{\partial w_2}{\partial \zeta} = \frac{1}{2G_m} \sum_{i=1}^{\infty} \cos k_i \zeta \left[a_{0i} K_0(k_i \xi) + a_{1i} (k_i \xi K_1(k_i \xi) - 4(1-\nu_m) K_0(k_i \xi)) \right] \quad (40)$$

$$u_2 = -\frac{1}{2G_m} \frac{A_1}{\xi} + \frac{1}{2G_m} \sum_{i=1}^{\infty} \cos k_i \zeta \left(a_{0i} \frac{K_1(k_i \xi)}{k_i} + a_{1i} \xi K_0(k_i \xi) \right) \quad (41)$$

These stresses, strains, and displacements were calculated by substituting the appropriate stress function into one of Eqs (7)–(12) or Eqs (21)–(26) and then transforming into a dimensionless coordinate system with $\xi = r/r_1$ and $\zeta = z/r_1$. We defined some new constants (B_1 , B_2 , and B_3) and redefined the remaining constants all in terms of the original constants in Eqs (28) and (29). For use in dimensionless equations, we have also redefined k_i to be

$$k_i = \frac{2r_1 i \pi}{l} = \frac{i \pi}{\rho} \quad (42)$$

where $\rho = l/(2r_1)$ is the aspect ratio of the fragment. Finally, we note that the displacements u_i and w_i are dimensionless displacements (u_{actual}/r_1 or w_{actual}/r_1).

The radial stress, axial strain, and radial displacement in the fiber all have a term in the Fourier expansion summation that does not involve a Bessel function. These non-Bessel function terms arise from the leading terms in the fiber stress function. These leading terms give stresses and strains that are independent of ζ and also stresses and strains that vary as ζ^2 . Because our analysis involves term-by-term equating of the coefficients of the Fourier expansion, we *must* resolve the ζ^2 terms into a Fourier series. The constant parts of these series are kept with the ζ -independent stresses. The Fourier parts are added to the Fourier expansion summation. These non-Bessel function terms in the Fourier expansion are crucial to our analysis procedure. Without them, our method would be unable to yield a nonzero solution to the problem. With them, a solution is possible.

In the dimensionless coordinates, the fiber fragment extends from $-\rho$ to ρ . Inspection of the matrix shear stress, the matrix axial displacement, and the fiber shear stress show that

$$\tau_{rz,2}(\pm\rho) = 0 \quad w_2(\pm\rho) = 0 \quad \tau_{rz,1}(\pm\rho) = 0 \quad (43)$$

Thus the stress state exactly satisfies most of the boundary conditions. The single remaining boundary condition is $\sigma_{zz,1}(\pm\rho) = -1$. Because $\sigma_{zz,1}(\pm\rho)$ in Eq (31) is a function of ξ , this final boundary condition cannot be satisfied exactly. Instead, we satisfy it in the average or we satisfy $\langle\sigma_{zz,1}(\pm\rho)\rangle = -1$. Integrating $\sigma_{zz,1}$ over the cross-section gives the average axial stress in the fiber:

$$\langle\sigma_{zz,1}\rangle = B_2 + \frac{B_3d}{2} + \sum_{i=1}^{\infty} \cos k_i \zeta \left[b_{1i} \left(\frac{c}{s_1^2} - d \right) \frac{I_1(\beta_{1i})}{\beta_{1i}} + b_{2i} \left(\frac{c}{s_2^2} - d \right) \frac{I_1(\beta_{2i})}{\beta_{2i}} \right] \quad (44)$$

Thus we seek to satisfy

$$-1 = B_2 + \frac{B_3d}{2} + \sum_{i=1}^{\infty} (-1)^i \left[b_{1i} \left(\frac{c}{s_1^2} - d \right) \frac{I_1(\beta_{1i})}{\beta_{1i}} + b_{2i} \left(\frac{c}{s_2^2} - d \right) \frac{I_1(\beta_{2i})}{\beta_{2i}} \right] \quad (45)$$

Because the fiber stress function satisfies $\nabla_1^2 \nabla_2^2 \Psi = 0$ and the matrix stress function satisfies $\nabla^4 \chi = 0$, the stress state derived from those stress functions satisfies equilibrium and compatibility at all locations. From above, we see that the stresses satisfy the matrix boundary conditions and fiber shear-stress boundary condition exactly. The single approximation is that we only satisfy the fiber axial-stress boundary condition in the average. The solution can be said to be exact except in regions very near the fiber ends. An exact solution would show stress singularities where the fiber crack tip meets the matrix. Our Fourier expansion solution cannot have mathematical singularities, but our solution does correctly show large stress concentrations near the crack tip. Very local to the crack tip the stresses increase as the number of terms in the Bessel-Fourier series increases. Slightly farther away from the crack tip, the stresses rapidly converge and become independent of the number of terms in the Bessel-Fourier series. Finally, we note that the fiber stress function does not reduce to the correct result for an isotropic fiber. Similar results for isotropic fibers, however, can be generated by using the new fiber stress function of

$$\Psi = A_{30}z^3 + A_{32}r^2z + A_{50} \left((2 - \nu_f)z^5 - \frac{15\nu_f}{8}r^4z - 5(1 - \nu_f)r^2z^3 \right) + \sum_{i=1}^{\infty} \sin k_i z (b_{1i}I_0(k_i r) + b_{2i}k_i r I_1(k_i r)) \quad (46)$$

where ν_f is the Poisson's ratio of the isotropic fiber.

The solution for a full fragmentation specimen can be constructed by piecing together individual solutions for each individual fiber fragment. Formally, such a solution only applies to specimens with periodic fiber breaks. If the breaks are not periodic, the solution will still obey boundary conditions, but it will include discontinuities in the matrix axial stress at the junctions between fiber fragments. Thus, this solution contains an additional approximation when applied to specimens with nonperiodic breaks.

Imperfect Interface

Most analyses of stress transfer from a matrix to a fiber resort to assuming a perfect interface [9–14]. A definition of a perfect interface is that σ_{rr} , τ_{rz} , u , and w are all continuous at $r = r_1$ or at $\xi = 1$. The goal of the fragmentation test and other interface tests, such as the pull-out test [19, 20] or microbond test [21, 22], is to measure interface properties. It is self-evident that analyses that assume a perfect interface will never be helpful in interpreting such tests. The assumption of a perfect interface predetermines the interface properties in the analysis and thus cannot be used to study the effect of varying those properties on experimental results. We must therefore include some model for an imperfect interface into our fragmentation test analysis.

The mathematician's approach to an imperfect interface is to relax interfacial continuity conditions and allow there to be discontinuities in σ_{rr} , τ_{rz} , u , and w [23]. In linear theories, the discontinuities are assumed to be linear functions of the interfacial stress state. In static loading conditions, stress equilibrium requires σ_{rr} and τ_{rz} to be continuous regardless of the quality of the interface. The remaining discontinuities in u and w are functions of the interfacial stresses. Hashin put this imperfect interface model into physical terms for composites [24, 25]. The interface in real composites is better described as an interface zone of finite dimension or an *interphase*. Within the interphase, the mechanical properties differ from both the fiber and the matrix. If the interphase plays a role in composite properties, then it must allow the fiber to displace relative to the matrix. Unfortunately, we are unlikely to have detailed information about the

thickness or the mechanical properties of the interphase. To make matters more complex, there might be a gradient of mechanical properties across the interphase. Adding an interphase zone with variable and probably unknown mechanical properties severely complicates our analysis of the fragmentation test. Hashin proposed collapsing the 3D interphase into a 2D interface [24, 25]. The effect of the interphase is modeled by allowing displacement discontinuities at the 2D interface that are linearly related to the stress in each displacement direction. Denoting interface discontinuities with square brackets (*e.g.*, $[u] = u_2(1, \zeta) - u_1(1, \zeta)$), a fiber interface reduces to

$$[u] = \frac{\sigma_{rr,1}(1, \zeta)}{D_n} = \frac{\sigma_{rr,2}(1, \zeta)}{D_n} \quad (47)$$

$$[w] = \frac{\tau_{rz,1}(1, \zeta)}{D_s} = \frac{\tau_{rz,2}(1, \zeta)}{D_s} \quad (48)$$

$$[v] = \frac{\tau_{r\theta,1}(1, \zeta)}{D_t} = \frac{\tau_{r\theta,2}(1, \zeta)}{D_t} \quad (49)$$

For axisymmetric stresses, $\tau_{r\theta} = [v] = 0$ and we only need to consider $[u]$ and $[w]$. The terms D_n and D_s are called interface parameters. A perfect interface is described by $D_n = D_s = \infty$; a disbonded interface is described by $D_n = D_s = 0$; intermediate values describe an imperfect interface. It is important to recognize that collapsing the interphase to a 2D interface does not mean we are ignoring the reality of an interphase. Instead, we are using a mathematical trick that lumps the effect of the interface into two interface parameters — D_n and D_s . In principle, D_n and D_s could be calculated for an interphase if its mechanical properties and dimensions were known. Some sample calculations for planar interfaces are given in Ref. [23]. For example, consider an interphase of thickness t_i on a fiber. The discontinuity in axial displacement across the interphase is $r_1[w]$ (w here is a dimensionless displacement). A simple one-dimensional analysis for shear strain in the interphase gives

$$\gamma_{rz,i} = \frac{r_1[w]}{t_i} \quad (50)$$

Substituting the imperfect interface model for $[w]$ and assuming the interphase shear stiffness is G_i we find a physical interpretation for D_s as

$$D_s = \frac{r_1 G_i}{t_i} \quad (51)$$

Thus D_s has units of a modulus and is related to the *effective* shear stiffness of the interphase. This one-dimensional picture probably oversimplifies the physical meaning of D_s . D_s is better imagined as a measure of the ability of the interphase to transfer stress from the matrix back into the fiber.

In the fragmentation test, thermal shrinkage of the matrix and differential Poisson's contraction between the fiber and the matrix both promote compressive radial stresses [26]. Calculation of $\sigma_{rr}(1, \zeta)$ from the above stress analysis confirms that σ_{rr} is compressive over the entire interface except possibly for extremely small zones near the fiber ends. Under dominantly compressive radial stresses, the expression for $[u]$ implies a negative discontinuity or implies the matrix penetrates into the fiber. This situation illustrates a flaw in a linear imperfect interface. While negative discontinuities are permissible for tangential displacement, they should be forbidden for normal displacements. In the fragmentation test we have the fortunate simplification that σ_{rr} is compressive. We can thus prevent negative discontinuities in normal displacements while still using a linear theory simply by setting $D_n = \infty$. We are not assuming the interface is perfect in the radial direction; we are just exploiting the fact that σ_{rr} is compressive and therefore the quality of the interface in the radial direction should have no effect on fragmentation results.

The boundary conditions for the fragmentation test with an imperfect interface reduce to:

$$\sigma_{rr,1}(1, \zeta) = \sigma_{rr,2}(1, \zeta) \quad (52)$$

$$\tau_{rz,1}(1, \zeta) = \tau_{rz,2}(1, \zeta) \quad (53)$$

$$[u] = 0 \quad (54)$$

$$[w] = \int_0^\zeta (\varepsilon_{zz,2} - \varepsilon_{zz,1}) d\zeta = \frac{\tau_{rz,1}(1, \zeta)}{D_s} \quad (55)$$

$$\langle \sigma_{zz,1}(\pm\rho) \rangle = -1 \quad (56)$$

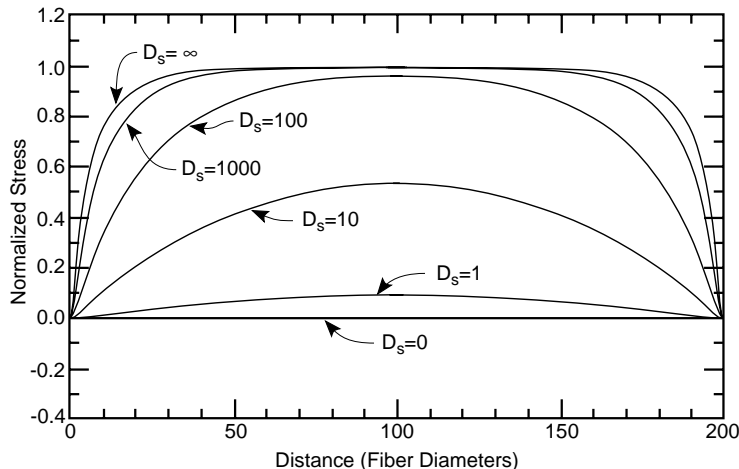


FIG. 2 — Sample calculation of the effect of an imperfect interface on the average axial tensile stress in an HM carbon fiber as a function of distance along the fiber for a fiber fragment that is 200 fiber diameters long. All stresses have been normalized to the far-field axial fiber stress of ψ_∞ . $D_s = \infty$ is a perfect interface.; $D_s = 0$ is a disbanded interface; intermediate D_s 's (in MPa) are imperfect interfaces.

These conditions are exactly enough conditions to determine all the constants in the stress functions in Eqs (28) and (29). The need for this result influenced the choice of the leading terms in the stress functions. The constants are determined by equating, term-by-term, the terms in the Bessel-Fourier series of each boundary condition. This process involves solving a 4×4 linear system for each term in the Bessel-Fourier series and one 4×4 linear system for the constant terms. These equations can easily and rapidly be solved on a personal computer.

For a sample calculation, we plot stress transfer from a high modulus (HM) carbon fiber to a room-temperature cured epoxy matrix (see fiber and matrix properties in Table 1). Figure 2 plots the average axial stress in the HM carbon fiber for various values of D_s . The stress has been normalized by dividing by ψ_∞ . For a perfect interface ($D_s = \infty$) the stress transfers back into the fiber in about 30 fiber diameters. Experimental results for stress transfer on the same fiber and matrix show stress transfer in about 50 fiber diameters [27, 28]. Our calculations for a perfect interface with no parameters are in qualitative agreement with experimental results. We note that stress transfer into anisotropic, high-modulus carbon fibers is considerably slower than into isotropic glass fibers. The slower transfer into carbon fibers is mostly a consequence of the higher modulus ratio between the fiber and the matrix [11, 15]. As D_s decreases, the stress transfer zone gets longer. As D_s approaches zero, the axial stress approaches zero, as it should for a disbanded interface. The specific value of D_s about 500 MPa gives a stress transfer zone of 50 fiber diameters which agrees exactly with experimental results [27, 28].

Comparison to Raman Experiments

Certain Raman bands in carbon fibers shift when the fiber is under stress [29]. Several investigators have used this shift to directly measure the stress in a carbon fiber embedded in a matrix (*e.g.*, Refs. [27–32]). Here we consider a specific set of experiments on a short HM carbon fiber embedded in a room-temperature cured epoxy [28]. The mechanical properties for the fiber and matrix are given in Table 1. The short fibers were embedded in the matrix and the stress in the fiber as a function of distance from the fiber end was measured at several levels of applied strain. Details about the experimental procedures are given in Ref. [28]. In this section we compare two experimental results to predictions. The two experimental results are stress transfer at low strain and stress transfer at high strain after evidence of interfacial damage.

The stress analysis in this paper is for a fragment that has broken away from a continuous fiber. The experimental results are for an isolated end of an embedded short-fiber, which is formally different than the end of a fragment from a continuous fiber. There is another consideration, however, that argues in favor of comparing the analysis to experiments on short fibers instead of experiments on fragmented fibers. To

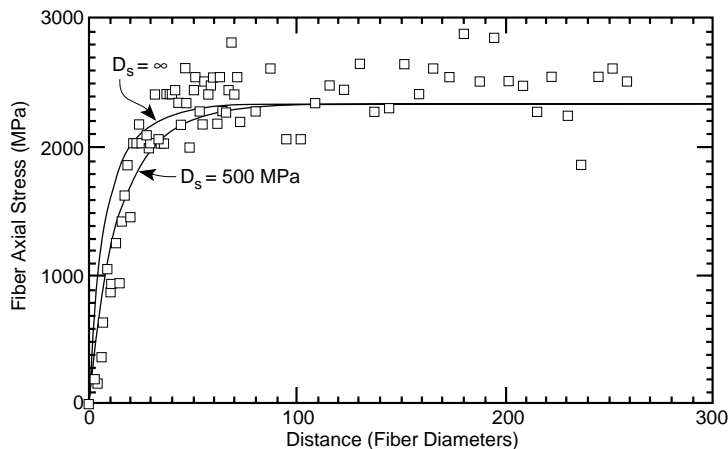


FIG. 3 — A comparison of Raman measurements of stress transfer at an applied strain of 0.6% to predictions using the Bessel-Fourier series. The $D_s = \infty$ curve is the prediction for a perfect interface. Setting $D_s = 500$ MPa gives a more accurate prediction of the stress transfer process.

make specimens with fiber fragments, it is necessary to embed a continuous fiber in a matrix and extend the specimen until the fiber begins to fragment. The first fragments do not appear until the applied strain exceeds the strain to failure of the fiber or around 0.8% strain for HM fibers. Thus, it is impossible to do experiments on fragments that have been loaded to less than 0.8% strain. If the fragmentation process itself causes interfacial damage, then it is also impossible to study “elastic” transfer from the matrix to the fiber. By elastic transfer, we mean stress transfer through an undamaged, although perhaps still imperfect, interface. To get some results in the elastic regime, it is preferable to do experiments on short-fiber specimens.

Figure 3 compares the Raman measurements of stress transfer at an applied strain of 0.6% to the predictions of the Bessel-Fourier series stress analysis. We began by assuming a perfect interface. The result in the $D_s = \infty$ curve shows that the predictions agree reasonably well with experimental results. The experimental stress transfer, however, is slightly slower than the predictions. By varying D_s , we found that $D_s = 500$ MPa agrees better with experimental results. Comparison to other experiments in the low-strain regime ($\varepsilon < 0.8\%$) [28] showed that they could all be fit well the same value of D_s . We claim that $D_s = 500$ MPa provides a useful measure of the quality of the interface between HM carbon fibers and the epoxy matrix.

Figure 4 shows experimental results at an applied strain of 1.0%. The stress transfer begins slowly, but at about 50 fiber diameters from the end undergoes a discontinuous change in slope. Comparison to FIG. 2 shows that no single value of D_s can predict such a change in stress transfer rate. Instead, we suggest that the high applied strain has caused a damaged zone in the vicinity of the fiber end. The damaged zone

TABLE 1 — Thermal and mechanical properties used for the fiber and the matrix.

Property	HM or T50 Carbon Fibers	Epoxy Matrix
Diameter ($2r_1$) (μm)	7	
Tensile Modulus (E_A or E_m) (GPa)	390	2.6
Transverse Modulus (E_T) (GPa)	14	
Axial Shear Modulus (G_A or G_m) (GPa)	20	0.97
Axial Poisson’s Ratio (ν_A or ν_m)	0.20	0.34
Transverse Poisson’s Ratio (ν_T)	0.25	
Axial CTE (α_A or α_m) ($10^{-6}/^\circ\text{C}$)	-0.36	40
Transverse CTE (α_T) ($10^{-6}/^\circ\text{C}$)	18	

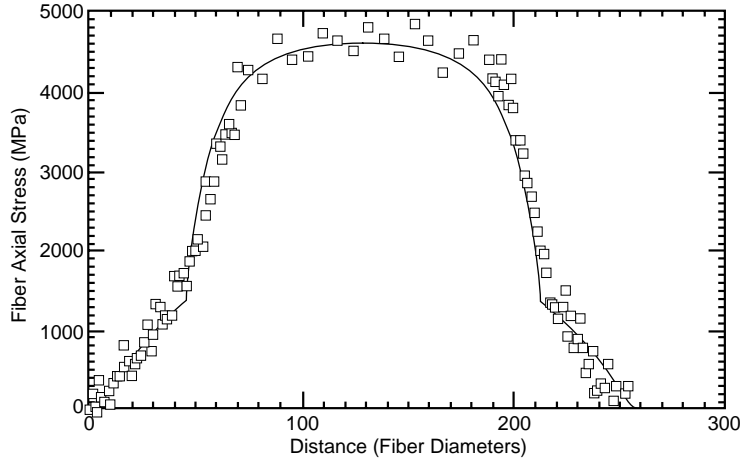


FIG. 4 — A comparison of Raman measurements of stress transfer at an applied strain of 1.0% to predictions using the Bessel-Fourier series. The predictions are for a two zone model with $D_s = 5$ near the fiber break and $D_s = 500$ in the central portion of the fiber.

could be caused by numerous events such as matrix cracking, matrix yielding, interfacial debonding, or fiber splitting. Whatever the cause of the damage, we claim its effect is to change the effective value of D_s near the fiber end. We thus propose a two-zone model as illustrated in FIG. 5. Within the damaged zone that extends a distance r_d from the fiber end, the interface is characterized by a low value of D_s . The stresses are found by analysis of a fragment of axial ratio ρ_1 which is equal to the axial ratio of the entire fragment. In the central portion of the fragment, the D_s value is high. The stresses are found by analyzing a fragment of length ρ_2 where ρ_2 is chosen such that the average axial fiber stress is continuous at the edge of the damaged zone. The two-zone model is only an approximate model because only the average fiber stress is continuous at the junction between the two zones. The axial and shear stresses in the matrix and the shear stress at the interface will be discontinuous. We believe the two-zone model still provides a useful model for stress transfer in the presence of a damaged interface.

Figure 4 compares predictions of the two-zone model to experimental results at an applied strain of 1.0%. The D_s value in the center of the fiber represents stress transfer across an undamaged interface. As such, it should be expected to be the same as the D_s value measured over the entire fiber fragment in low-strain experiments. We thus used $D_s = 500$ MPa for the central zone. The best-fit D_s for the damaged zone

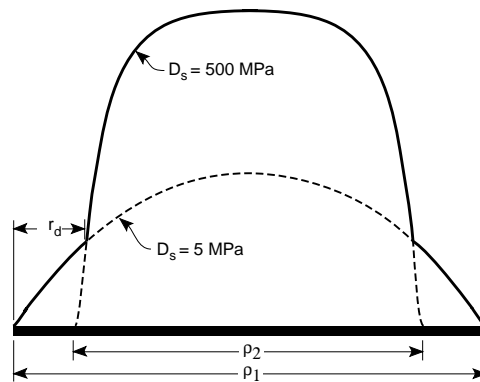


FIG. 5 — A simple two-zone model for predicting stress transfer in the presence of interfacial damage. The D_s value is low near the fiber ends and high in the middle of the fragment. r_d is the length of the damaged zone. The value of ρ_2 is chosen such that the average axial stress in the fiber is continuous at the edge of the damaged zone.

was $D_s = 5$ MPa. Using these two values of D_s and a damaged zone size of $r_d = 48$ fiber diameters, the analysis agrees well with experimental results. Note that the high strain experiments have less scatter than the low strain experiments because the absolute shifts in the Raman bands are larger. The $D_s = 500$ MPa result obtained by fitting the central portion of the fiber is perhaps more reliable than the similar result obtained by comparison to low-strain experiments. We also calculated the interfacial shear stresses and the octahedral shear stress in the matrix using the two-zone model. The interfacial shear stress agrees well with the Raman results [28]. The octahedral shear stress results suggest that the mechanism for interfacial damage is matrix yielding. In other words, the size of the damage zone used to fit the experiments in FIG. 4 coincides identically with the damage zone required to prevent the octahedral shear stress from ever exceeding the condition for matrix yielding.

Fragmentation Test Analysis

In the fragmentation test, a given fiber fragment is typically assumed to break into two smaller fragments when the stress in the fiber reaches the strength of the fiber at the length of the fragment. The peak stress in a fragment is always in the middle. The fragmentation test is thus described by the equation

$$\langle \sigma_{zz,1}(\zeta = 0) \rangle = \sigma_{ult}(l) \quad (57)$$

Inserting the Bessel-Fourier series analysis for $\langle \sigma_{zz,1}(\zeta = 0) \rangle$ and inverting gives fragment length or fiber break density ($= 1/l$) as a function of applied stress (σ_0) and temperature differential (T). In this section we compare predictions to experimental results. Unfortunately, many fragmentation results report only the critical length or the fiber break density after the fragmentation process ceases. To get more insight into the fragmentation process, it is preferable to have data at sub-critical lengths or data that gives fiber break density as a function of applied load [5, 6, 32]. Here we compare our predictions to experimental results by Huang and Young [32]. They measured fiber break density as a function of applied strain for high-modulus, PAN based, T50 carbon fibers in a room-temperature cured epoxy. The mechanical properties of the fiber and matrix are given in Table 1.

The fiber length-strength relation was empirically found to be linear on a semi-log plot. T50 fiber strength in GPa as a function of length in mm was measured to be [32]

$$\sigma_{ult}(l) = 3.75 - 0.817 \log l \quad (58)$$

Combining Eqs (57) and (58) and assuming the interface is characterized by a single value of D_s , we can predict the fragmentation process as a function of D_s . The results are in FIG. 6. At low break density, the experimental results can be predicted with a range in D_s . No single, value of D_s , however, can predict all experimental results. The experimental results bend over more quickly than any of the theoretical curves. Analogous to the Raman results, we suggest that the fragmentation results at high crack density should be modeled with a two-zone model instead of a single value of D_s .

To conduct a two-zone analysis of the fragmentation test we need to know D_s in the central portion of the fiber, know D_s near the fiber break, and have enough information about the interfacial damage process to predict r_d as a function of applied strain. D_s in the central zone reflects stress transfer across an undamaged, although possibly imperfect, interface. We find this value from the results at the lowest break densities. From FIG. 6, the value of D_s that fits the results best without ever dropping below the results is $D_s = 100$ MPa. D_s in the damaged zone influences the rate at which the predictions level off at high strain. For now, we treat it as an adjustable parameter.

An important part of analyzing fragmentation tests is understanding the interfacial damage process and predicting r_d as a function of applied strain. We did not have specific information about interfacial damage in these specimens. To guess a damage mechanism, we examined the interfacial stresses for applied strains at the onset of damage or at the onset of deviations from the predictions when $D_s = 100$ MPa. We noticed that the octahedral stress, defined as

$$\tau_{oct} = \frac{1}{3} \sqrt{(\sigma_{rr} - \sigma_{zz})^2 + (\sigma_{rr} - \sigma_{\theta\theta})^2 + (\sigma_{zz} - \sigma_{\theta\theta})^2 + 6\tau_{rz}^2}, \quad (59)$$

predicted no yielding for low strains, but predicted matrix yielding for strains above the onset of damage. In other words, $\tau_{oct} \approx \frac{\sqrt{3}}{3} \sigma_y$, where $\sigma_y = 75$ MPa is the tensile yield stress of the matrix [32], at the onset of

damage. We therefore suggest that interfacial damage in these specimens was controlled by matrix yielding at the interface. For any given D_s values in the damaged zone and the central zone, it is a simple calculation to plot τ_{oct} along the interface for various values of r_d . For each applied strain, we selected r_d such that the interfacial value of $\frac{3\tau_{oct}}{\sqrt{2}}$ was lower than the tensile yield stress of the matrix. One complication of this analysis was that for a finite number of terms in the Bessel-Fourier series, there were oscillations in τ_{oct} . To average out the high-frequency oscillations, we looked at the average value of τ_{oct} over a small region at the tip of the damaged zone. We averaged τ_{oct} over a region that was 2% of the fiber length. This region size was selected empirically; it was the smallest region for which the prediction of r_d as a function of applied strain was observed to independent of the number of terms used in the Bessel-Fourier series.

The results of predicting fragmentation results using a two-zone model are given in FIG. 7. We assumed $D_s = 100$ MPa in the central zone, that the matrix tensile yield stress is 75 MPa, and that the interfacial damage process is controlled by matrix yielding. By fitting the experimental data, we found $D_s = 20$ –30 MPa in the damaged zone. The predictions agree well with the experimental results. Although the fit may not be unique, we have used fragmentation data to extract three pieces of information about the interface. $D_s = 100$ MPa in the central zone characterizes stress transfer across an undamaged interface. $D_s = 20$ –30 MPa in the damaged zone characterizes stress transfer across a damaged interface. The yield stress of 75 MPa characterizes the failure process at the interface.

Discussion

Analysis of both Raman experiments and fragmentation experiments makes it possible to determine D_s in the “elastic” regime and D_s for a damaged interface. In Raman experiments, the elastic D_s can be determined from either low-strain experiments or from the central portion of high-strain experiments. The damage-zone D_s can be determined from results near the fiber end in high-strain experiments. In the fragmentation test, the elastic D_s can be determined from the low break-density results. The damage-zone D_s can be determined from the critical length results or from the rate at which the break density curve levels off. Both values of D_s give information about the interface, but we suggest that the elastic D_s is much more relevant to real laminates than the damage-zone D_s . Real laminates are not fragmented into critical length fragments. Thus stress transfer in real laminates is controlled by the elastic D_s . To the extent that the interface plays a role in laminate properties, its effect should be determined by the elastic D_s and much less influenced by the damage-zone D_s .

We note that most work using the fragmentation test reports only the critical length or the corresponding interfacial shear stress. Because critical length is controlled by the damage-zone D_s , it is possible that critical length results are not relevant to the role of the interface in real laminates. The flaw of the fragmentation test

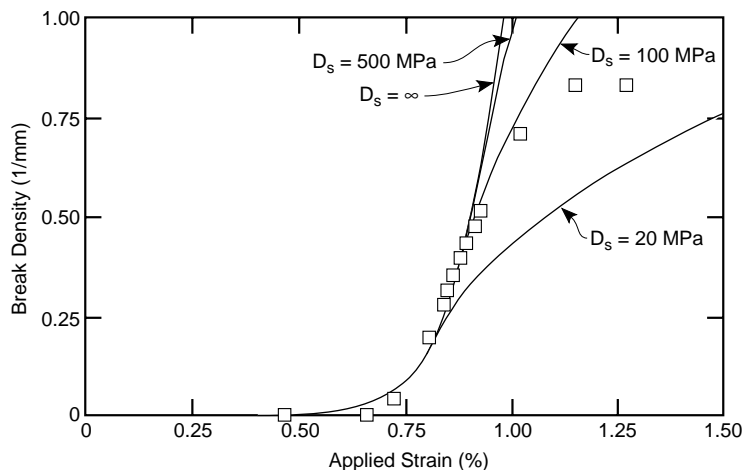


FIG. 6 — Comparison between fragmentation experiments on T50 carbon fibers in a room-temperature cured epoxy matrix and theoretical predictions assuming the interface can be characterized by a single value of D_s

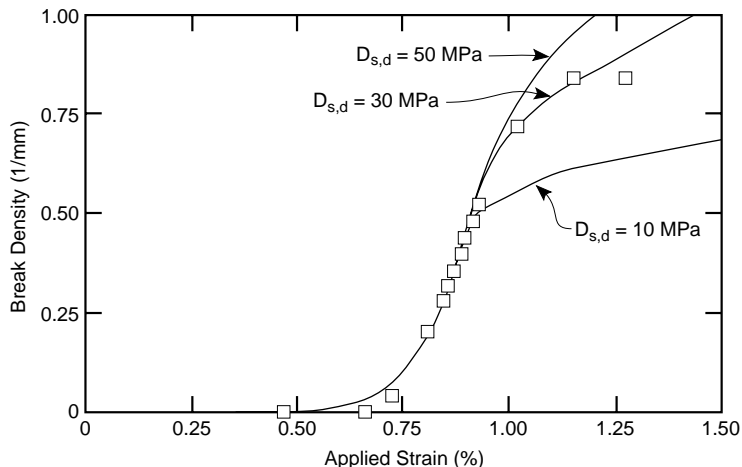


FIG. 7 — Comparison between fragmentation experiments on T50 carbon fibers in a room-temperature cured epoxy matrix and theoretical predictions using a two-zone model. $D_s = 100$ MPa in the central zone; $D_{s,d}$ (or D_s in the damaged zone) equal to various values; the size of the damaged zone was assumed to be controlled by matrix yielding at a tensile yield stress of 75 MPa.

is not in the experiment itself, but rather in the idea that only critical length is important. The fragmentation test can be fixed by doing experiments at sub-critical length or at low break density [5, 6, 32]. The analysis in this paper can be used to extract the elastic D_s from such experiments.

Complete modeling of the fragmentation test requires modeling the interfacial damage process. Here we assumed a matrix yielding process based on the interfacial octahedral shear stress. An advantage of the Bessel-Fourier series stress analysis is that we can calculate all the components interfacial stress and therefore do a realistic interfacial yielding analysis. Some previous analyses have assumed shear yielding and examined only the interfacial shear stress. Because interfacial shear stress is zero at the fiber break, a simple shear yielding model is inadequate. It predicts there will be no yielding near the fiber break. In contrast, the octahedral shear stress is not zero. Because of large radial, hoop, and axial stresses near the fiber break, the octahedral shear stress is nonzero and yielding is naturally predicted to extend from the fiber break along the interface. A realistic analysis of interfacial yielding must account for the important contributions of normal stresses to the yielding process.

We do not claim that matrix yielding is the damage process in all fragmentation experiments. Other damage modes such as matrix cracking, fiber cohesive failure, frictional sliding, or interfacial debonding might occur instead. In principle, the Bessel-Fourier series stress analysis could be used to develop fragmentation models based on other interfacial damage processes. For example, optical observation of the interface with glass fibers in certain matrices suggests interfacial debonding as the fragmentation process proceeds [33]. We are in the process of predicting such interfacial damage by calculating the energy release rate for growth of an interfacial debond. The debonding could be predicted to grow when that energy release rate exceeds the interfacial toughness. Perhaps the fragmentation test can then be used to measure interfacial toughness.

In principle, a fragmentation test as a function of applied strain can be used to extract information about stress transfer across damaged or undamaged interfaces and about the interfacial damage process. Practically speaking, however, there are too many variables to be guaranteed of finding accurate information. A preferred approach is to couple fragmentation experiments with independent experiments on the same specimens. One could, for example, couple fragmentation experiments with Raman spectroscopy experiments. The Raman experiments could be used to directly measure the elastic D_s and the damage-zone D_s . The fragmentation experiments could input these parameters and focus on the interfacial damage process. Modeling the interfacial damage could further be coupled with optical microscopy to insure that the proposed failure models are realistic.

Acknowledgements

This work was supported in part by a grant from the Mechanics of Materials program at NSF (CMS-9401772) and in part by a Fulbright Fellowship for one of the authors (J. A. Nairn). We thank R. J. Young for providing the fragmentation test experimental results.

References

- [1] Wadsworth, N. J. and I. Spilling, "Load Transfer from Broken Fibres in Composite Materials," *Br. J. Appl. Phys. (J. Phys. D.)*, Vol. 1, 1968, pp. 1049–1058.
- [2] Fraser, A. A., F. H. Ancker, and A. T. DiBenedetto, "A Computer Modeled Single Filament Technique for Measuring Coupling and Sizing Effects in Fiber Reinforced Composites," *Proc. 30th Conf. SPI Reinforced Plastics Div.*, Vol. Section 22-A, 1975, pp. 1–13.
- [3] Drzal, L. T., M. J. Rich, and P. F. Lloyd, "Adhesion of Graphite Fibers to Epoxy Matrices: I. The Role of Fiber Surface Treatment," *J. Adhesion*, Vol. 16, 1983, pp. 1–30.
- [4] Bascom, W. D. and R. M. Jensen, "Stress Transfer in Single Fiber/Resin Tensile Tests," *J. Adhes.*, Vol. 19, 1986, pp. 219–239.
- [5] Wagner, H. D. and A. Eitan, "Interpretation of the Fragmentation Process Phenomenon in Single-Filament Composite Experiments," *Appl. Phys. Lett.*, Vol. 14, 1990, pp. 1965–1967.
- [6] Yavin, B., H. E. Gallis, J. Scherf, A. Eitan, and H. D. Wagner, "Continuous Monitoring of the Fragmentation Phenomenon in Single Fiber Composite Materials," *Polym. Comp.*, Vol. 12, 1991, pp. 436–446.
- [7] Kelly, A. and W. R. Tyson, "Tensile Properties of Fibre-Reinforced Metals: Copper/Tungsten and Copper/Molybdenum," *J. Mech. Phys. Solids*, Vol. 13, 1965, pp. 329–350.
- [8] Lacroix, Th., B. Tilmans, R. Keunings, M. Desaeger, and I. Verpoest, "Modeling of Critical Fibre Length and Interfacial Debonding in the Fragmentation Testing of Polymer Composites," *Comp. Sci. & Tech.*, Vol. 43, 1992, pp. 379–387.
- [9] Muki, R. and E. Sternberg, "On the Diffusion of an Axial Load From an Infinite Cylindrical Bar Embedded in an Elastic Medium," *Int. J. Solids Structures*, Vol. 5, 1969, pp. 587–605.
- [10] Muki, R. and E. Sternberg, "Elastostatic Load-Transfer to a Half-Space from a Partially Embedded Axially Loaded Rod," *Int. J. Solids Struct.*, Vol. 6, 1970, pp. 69–90.
- [11] Muki, R. and E. Sternberg, "Load-Absorption by a Discontinuous Filament in a Fiber-Reinforced Composite," *Z. angew. Math. Phys.*, Vol. 22, 1971, pp. 809–824.
- [12] Fowler, G. F. and G. B. Sinclair, "The Longitudinal Harmonic Excitation of a Circular Bar Embedded in an Elastic Half-Space," *Int. J. Solids Structures*, Vol. 14, 1978, pp. 999–1012.
- [13] Rajapakse, R. K. N. D. and A. H. Shah, "On the Longitudinal Harmonic Motion of An Elastic Bar Embedded in an Elastic Half Space," *Int. J. Solids Structures*, Vol. 23, 1987, pp. 267–285.
- [14] Pak, R. Y. S., "On the Flexure of a Partially Embedded Bar Under Lateral Loads," *J. Appl. Mech.*, Vol. 56, 1989, pp. 263–269.
- [15] Mbanefo, U. and R. A. Westman, "Axisymmetric Stress Analysis of a Broken, Debonded Fiber," *J. Appl. Mech.*, Vol. 57, 1990, pp. 654–660.
- [16] Pak, R. Y. S. and A. T. Gobert, "Axisymmetric Problems of a Partially Embedded Rod with Radial Deformation," *Int. J. Solids Structures*, Vol. 39, 1993, pp. 1745–1759.
- [17] Lekhnitski, S. G., *Theory of an Anisotropic Body*, MIR Publishers, Moscow, 1981.
- [18] Love, A. E. H., *A Treatise on the Mathematical Theory of Elasticity*, Dover Publications, New York, 1944.
- [19] Penn, L. S. and E. R. Bowler, "A New Approach to Surface Energy Characterization for Adhesive Performance Prediction," *Surf. Interf. Anal.*, Vol. 3, 1981, pp. 161–164.

- [20] Piggott, M. R., P. S. Chua, and D. Andison, "The Interface Between Glass and Carbon Fibers and Thermosetting Polymers," *Polym. Comp.*, Vol. 6, 1985, pp. 242–248.
- [21] Miller, B., P. Muri, and L. Rebenfeld, "A Microbond Method for Determination of the Shear Strength of a Fiber/Resin Interface," *Comp. Sci. & Tech.*, Vol. 28, 1987, pp. 17–32.
- [22] Gaur, U. and B. Miller, "Microbond Method for Determination of the Shear Strength of a Fiber/Resin Interface: Evaluation of Experimental Parameters," *Comp. Sci. & Tech.*, Vol. 34, 1989, pp. 35–51.
- [23] Martin, P. A., "Boundary Integral Equations for the Scattering of Elastic Waves by Elastic Inclusions with Thin Interface Layers," *J. Nondestructive Evaluation*, Vol. 11, 1992, pp. 167–174.
- [24] Hashin, Z., "Thermoelastic Properties of Fiber Composites With Imperfect Interface," *Mech. of Materials*, Vol. 8, 1990, pp. 333–348.
- [25] Hashin, Z., "Composite Materials with Interphase: Thermoelastic and Inelastic Effects," in *Inelastic Deformation of Composite Materials*, ed., G. J. Dvorak, Springer-Verlag, New York, 1990, pp. 3–34
- [26] Nairn, J. A., "A Variational Mechanics Analysis of the Stresses Around Breaks in Embedded Fibers," *Mech. of Materials*, Vol. 13, 1992, pp. 131–154.
- [27] Melanitis, N., C. Galiotis, P. L. Tetlow, and C. K. L. Davies, "Interfacial Shear Stress Distribution in Model Composites Part 2: Fragmentation Studies on Carbon Fibre/Epoxy Systems," *J. Comp. Mat.*, Vol. 26, 1992, pp. 574–610.
- [28] Melanitis, N., C. Galiotis, P. L. Tetlow, and C. K. L. Davies, "Monitoring the Micromechanics of Reinforcement in Carbon Fibre/Epoxy Resin Systems," *J. Mat. Sci.*, Vol. 28, 1993, pp. 1648–1654.
- [29] Robinson, I. M., M. Zakikhani, R. J. Day, R. J. Young, and C. Galiotis, "Strain Dependence of the Raman Frequencies for Different Types of Carbon Fibres," *J. Mat. Sci. Lett.*, Vol. 6, 1987, pp. 1212–1214.
- [30] Schadler, L. S., C. Laird, N. Melanitis, C. Galiotis, and J. C. Figueroa, "Interfacial Studies on Carbon/Thermoplastic Model Composites Using Laser Raman Spectroscopy," *J. Mat. Sci.*, Vol. 27, 1992, pp. 1663–1671.
- [31] Melanitis, N., C. Galiotis, P. L. Tetlow, and C. K. L. Davies, "Interfacial Shear Stress Distribution in Model Composites: The Effect of Fiber Modulus," *Composites*, Vol. 24, 1993, pp. 459–466.
- [32] Huang, Y. and R. J. Young, "Analysis of the Fragmentation Test for Carbon Fibre/Epoxy Model Composites Using Raman Spectroscopy," *Comp. Sci. & Tech.*, 52, 1994
- [33] Wagner, H. D., J. A. Nairn, and M. Detassis, "Toughness of Interfaces from Initial Fiber-Matrix Debonding in a Single-Fiber Composite Fragmentation Test," *Applied Comp. Mater.*, Vol. 2, 1995, pp. 107–117.